ELSEVIER

Journal of Molecular Catalysis A: Chemical 162 (2000) 275–285

JOURNAL OF MOLECULAR CATALYSIS A: CHEMICAL

www.elsevier.com/locate/molcata

# Characterization of CuO/ZnO under oxidizing conditions for the oxidative methanol reforming reaction

T.L. Reitz [a,*], S. Ahmed [b], M. Krumpelt [b], R. Kumar [b], H.H. Kung [a]

[a] *Department of Chemical Engineering, Northwestern University, Evanston, IL 60208, USA*

[b] *Chemical Technology Division, Argonne National Laboratory, 9700 S. Cass Ave., Bldg. 205, Argonne, IL 60439, USA*

**Abstract**

Catalytic generation of hydrogen by the reaction of methanol with oxygen in the presence of steam over an industrial copper–zinc oxide catalyst was studied. Under differential oxygen conversion conditions, the catalyst remained in an oxidized state, and the main reaction was oxidation of methanol to carbon dioxide and water. The activity was proportional to the copper oxide surface area. The methanol consumption rate had a small positive order in methanol and oxygen (0.18th order) and was suppressed by water. The catalyst deactivated with time on stream due to agglomeration of copper oxide. As the reactor temperature increased, the rate of methanol oxidation increased, the oxygen conversion became very high, and the catalyst away from the reactor entrance became reduced. Then, a significant rate of hydrogen production was observed.


*Keywords:* CuO/ZnO; Oxidizing condition; Oxidative methanol reforming reaction

## 1. Introduction

Recently, there have been substantial efforts to investigate alternative propulsion systems for automobiles. The desire to conserve oil reserves, and concerns over health issues and climate change are presented as reasons for decreasing emphasis on the use of the internal combustion engine, [1–4]. Fuel cells are being reinvestigated as a potential alternative. Presently, the most viable candidate for automobile applications is the hydrogen fuel cell incorporating a proton exchange membrane. Because of safety and infrastructure considerations, onboard $H_2$ generation, by reforming a liquid fuel, is being extensively investigated for commercialization. Among the liquid fuels investigated for potential reforming feedstock, methanol has shown promise because of the ease of handling, low cost, and high-energy content [5,6].

The steam reforming of methanol to $H_2$ has been successfully demonstrated [7–11]. Due to the endothermicity of the reaction, significant heat is required in order to maintain the methanol reforming reaction (Eq. (1)). As a result, heat required for the steam reforming reaction would have to be supplied by combustion of methanol, residual hydrogen from the fuel cell, or other fuel external to the reformer. Additionally, copper catalysts display significant reforming activity only after a complete reductive pretreatment. Therefore, sequestration of the catalyst bed between usage cycles also represents a significant drawback to methanol steam reforming for automobile applications.

* Corresponding author.

1381-1169/00/$ - see front matter 
PII: S1381-1169(00)00296-X

A second catalytic technique, oxidative methanol reforming (OMR), involves producing $H_2$ from methanol and water while cofeeding with $O_2$. The ratio of the three reactants can vary and are often chosen such that the overall reaction is thermal–neutral or only modestly exothermic. In essence, the heat necessary to maintain steam reforming of methanol is supplied by methanol oxidation (Eq. (2)) in the reactor. The stoichiometry of the OMR reaction at an oxygen/methanol ratio of 0.25 is shown as Eq. (3).

$$CH_3OH + H_2O = CO_2 + 3H_2$$

$$\Delta H^0_{298°C} = 130.9\,kJ/mol \quad (1)$$

$$CH_3OH + \frac{3}{2}O_2 = CO_2 + H_2O$$

$$\Delta H^0_c = -726.6\,kJ/mol \quad (2)$$

$$CH_3OH + 0.25O_2 + 0.5H_2O = CO_2 + 2.5H_2$$

$$\Delta H^0_{298°C} = -12.0\,kJ/mol \quad (3)$$

While steam reforming of methanol for $H_2$ production has been studied extensively [7–11], there are significantly fewer investigations of the OMR reaction. The addition of $O_2$ to the steam reforming reaction was initially studied by Huang et al. [12,13] who determined the kinetics of the OMR reaction over a reduced catalyst for high conversions. These authors suggested that the OMR rate could be modeled by considering a two-step sequence where the overall reaction rate could be determined by the sum of partial oxidation and steam reforming rates. For the purposes of arriving at a rate expression, a reaction mechanism and a rate-determining step were assumed based upon the reaction scheme proposed by Wachs and Madix [14] for formaldehyde oxidation. A Langmuir–Hinshelwood expression was then developed to model the data under high oxygen conversion conditions.

Alejo et al. [15] investigated the partial oxidation of methanol in the absence of steam over copper containing catalysts. $O_2$ conversion was found to be a significant function of temperature with nearly complete conversion occurring by 488 K with $H_2$ and CO selectivity a strong function of residence time. Activation energy was observed to vary depending upon copper content from 71 kJ/mol to over 482 kJ/mol. CO selectivities, however, were higher than that reported for steam reforming and the rate of partial oxidation was found to be a strong function of copper content. ZnO- and $ZrO_2$-supported Pd catalysts were also found to be highly selective for methanol partial oxidation to CO, $CO_2$ and $H_2$ [16,17].

Kumar et al. [5,6] examined a variety of catalyst systems for OMR and determined unreduced $CuO/ZnO/Al_2O_3$ to be highly active and selective for $H_2$ production. Product compositions of greater than 50% ($H_2$ dry), while maintaining less than 1% CO, were observed for high methanol conversions. Additionally, the exothermic nature of the reaction allowed for rapid reformer startup of less than 200 s. Rapid responses to load changes, necessary for automotive applications, were also observed.

Reitz et al. [18] concluded that an operational $CuO/ZnO/Al_2O_3$ OMR bed consists of regions with activity varying based on the oxidation state of the copper catalyst. When conversions of $O_2$ are low, the copper catalyst remains in the oxidized form. Under these conditions, the combustion of methanol was found to be dominant with only minor selectivity to $H_2$. For higher $O_2$ conversions, the catalyst bed temperature increased as a result of the exothermic nature of the combustion reaction. Eventually, the temperature increased uncontrollably until complete conversion of $O_2$ occurred and the catalyst was shown to be in the reduced state. The consequence of this run-away was that the resulting product distribution, at complete $O_2$ conversion, changed dramatically, with $H_2$ becoming the dominant product.

Deactivation of the $CuO/ZnO/Al_2O_3$ system during the OMR reaction represents one significant obstacle to technical implementation. At present, the exact cause of deactivation is not known because of lack of information about the surface area of the active phase, presumably CuO. Currently, the standard method for determining the activity and performance of copper containing catalysts is with a reductive pretreatment. Once the catalyst has been completely reduced, the surface area of $Cu^0$ can be determined by $N_2O$ chemisorption, [19–23]. Bulk reduction of the sample, however, is likely to result in significant reconstruction of the CuO particles. Thus, the technique is not completely appropriate for

the OMR reaction since it has been shown that, under differential oxidizing conditions, the dominant phase of copper is in the oxidized state, [18].

The objective of this work is to examine the OMR reaction over a commercial $CuO/ZnO/Al_2O_3$ catalyst. Of particular interest is to examine the reaction kinetics and the deactivation phenomenon observed under differential oxidizing conditions, which has not been studied in detail before. A reaction network and kinetic information for the oxidizing region of the OMR catalyst system are also presented.

## 2. Experimental

### 2.1. Kinetic experiments

Kinetic experiments were performed by placing a powder catalyst of $CuO/ZnO/Al_2O_3$ diluted in SiC (ElectroAbrasives, 120–170 mesh), into a fused silica microreactor operating in a steady state flow system. The catalyst was a commercial low-temperature shift catalyst, BASF K3-110 (120–170 mesh), consisting of 40 wt.% CuO, 40% ZnO, and 20% $Al_2O_3$ as reported by the vendor. Methanol and water were supplied by saturating $N_2$ and $O_2$ (Matheson UHP) carriers, respectively, in two sets of jacketed saturators maintained by external temperature baths. The flow rates were kept at 100 ml/min (STP) total flow by Brooks model 5850E mass flow controllers. The feed composition consisted of 10–40% methanol, 1–12% $O_2$, 10–30% $H_2O$, 2.5% $CH_4$ (as a tracer), and the balance $N_2$. The temperature was varied from 180°C to 225°C and monitored by use of a thermocouple in a thermocouple well placed in the catalyst bed. The residence time was varied by adjusting the catalyst weight from 10 to 50 mg diluted with 450–490 mg of SiC. Gas phase concentrations were determined by on-line GC analysis (HP 6890) using two TCD detectors incorporating a 8′, 1/8″ OD HayeSep Q, ($CH_3OH$, $H_2O$, $CO_2$ and HCOOH using He as a carrier), and a 10′, 1/8″ OD molecular sieve 13× column, ($O_2$, $N_2$, CO, $H_2$ using Ar as a carrier), for gas separations. Minor oxygenate concentrations were determined by use of a HP 5710A GC with a FID detector monitoring the HayeSep Q separated effluent from the HP 6890 TCD detector. A schematic description of the flow system is shown as Fig. 1. Mass balance closure generally exceeded 98% and reactant conversions where calculated using Eq. (4), defined for oxygen asanjo

$$O_2 \text{ conversion} = \left[ \frac{\sum_i \nu_i [P_i]}{\sum_i \nu_i [P_i] + 2[O_2]} \right]_{\text{ext}} . \qquad (4)$$

Where $\nu_i$ is the number of O atoms in a molecule of product $i$. An analogous definition can be written for

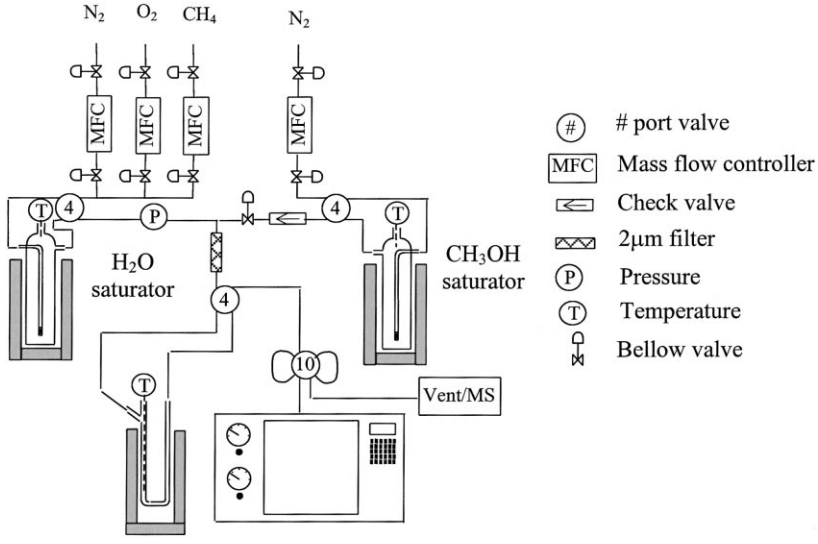


Fig. 1. System diagram for activity determination.

methanol. The products include $H_2$, $CO_2$, CO, $H_2O$, $CH_2O$, HCOOH and $CH_3OCH_3$. Product distributions are reported as a molar percentage of the total product concentration unless otherwise specified.

### 2.2. Catalyst characterization

Temperature programmed reaction (TPR) results were obtained in a flow apparatus with a fused silica microreactor. Gas flows of 60 ml/min consisting of 5% $H_2$/Ar (Matheson), were controlled by a Brooks Model 5850E mass flow controller. The furnace temperature was adjusted with a temperature controller (Omega Engineering) to maintain a constant ramp rate of 5 K/min. The oxygen impurity in the $H_2$/Ar feed was scrubbed by a MnO trap regenerated periodically by $H_2$ treatment at 450°C. Water generated during each TPR run was removed by a molecular sieve trap. A TCD detector, with output to a computer was used to monitor $H_2$ uptake. Pulses of 1 $cm^3$ UHP Ar (Matheson) were injected periodically during each run for calibration of the TCD signal. The system was calibrated by reducing CuO samples in $H_2$/Ar with mass balance closure of greater than $98 \pm 2\%$. Conditions of each run were controlled in order to optimize the TPR signal by adjusting the characteristic number $K$ (Eq. (5)), to below 200 $s^{-1}$ according to Monti and Baiker [24–27].

$$K = \frac{S_o}{VC_o}\,[=]\,s^{-1}, \tag{5}$$

where $S_o$ is the quantity of reducible species in the sample [=] μmol; $V$ is the volumetric flow rate [=] ml/s; $C_o$ is the initial $H_2$ content in the feed [=] μmol/ml.

$N_2$ BET surface area determination was obtained on a Coulter OmniSorb 360 at 77 K assuming a molecular cross-section of 0.164 nm. The samples were first outgassed at 225°C for 2 h under high vacuum. CuO surface area was determined by partial reduction in a flowing stream of 5% $H_2$/Ar for 60 min at 100°C, a temperature determined by a calibration described later. After 60 min, the system was purged in He and heated to 225°C. Pulses of 1 ml $O_2$ (STP) were then injected over the catalyst and uptake was determined by a TCD detector. Pure CuO was used to calibrate the procedure by comparing the results to the BET surface area. The porous copper oxide was prepared by precipitation of the nitrate salt with $NaHCO_3$. After washing to remove the $Na^+$, the filter cake was then dryed at 100°C for 24 h then calcined in air at 350°C for 6 h.

SEM data was obtained on a Hitachi 4500 FE-SEM apparatus. Powder XRD patterns were obtained with a Rigaku Geigerflex XRD diffractometer with Ni filtered $CuK_\alpha$ radiation, ($\lambda = 0.15418$ nm). Scans were generally performed from 10–80° $2\theta$ in 0.05° increments for 2 s count times. The Scherrer equation was used to estimate crystallite sizes using the FWHM for CuO (111) and ZnO (100) at 38.8° and 31.8°, respectively.

## 3. Results and discussion

### 3.1. Characterization of $CuO/ZnO/Al_2O_3$

In order to determine the condition to measure CuO surface area in $CuO/ZnO/Al_2O_3$, a calibration curve was prepared using pure CuO. Fresh samples of CuO were treated in 5% $H_2$/Ar at various temperatures for 60 min. After purging the catalyst in He at 225°C, the uptake of $O_2$ by the samples were determined. The uptake curves for the pure CuO and the $CuO/ZnO/Al_2O_3$ are reported in Fig. 2. For both samples, a small plateau in the $O_2$ uptake curve was observed for the samples reduced around 100°C. If this value was assumed to be due to reoxidation of the reduced copper surface from metal

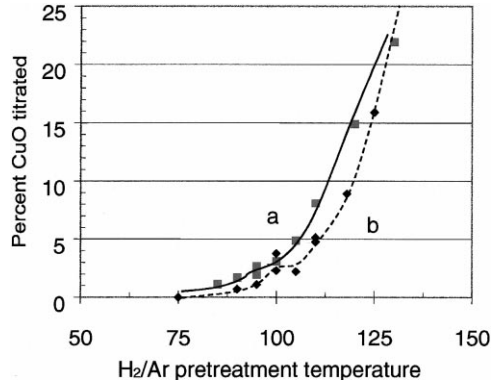


Fig. 2. CuO surface titration (a) pure CuO, (b) $CuO/ZnO/Al_2O_3$.

Table 1
Material properties of $CuO/ZnO/Al_2O_3$, BASF K3-110

| Parameter | Value |
|---|---|
| BET surface area [ = ] $m^2/g$ | $109 \pm 3$ |
| Pore volume [ = ] ml/g | $0.28 \pm 0.01$ |
| Average CuO particle size, A | $50 \pm 10$ |
| Average ZnO particle size, A | $40 \pm 10$ |
| CuO surface area [ = ] $m^2/g$ | $11 \pm 3.5$ |

to cupric oxide, the surface area of copper oxide was determined to be $29.0 \pm 3$ $m^2/g$, assuming a CuO molecule occupies $11.6 \cdot^2$ [28,29]. This is in reasonable agreement with the BET surface area of $20 \pm 2$ $m^2/g$. For the fresh-untreated $CuO/ZnO/Al_2O_3$ sample, the oxygen uptake at the plateau at 100–110°C corresponded to $3.6 \pm 1.4\%$ of the CuO titrated (Fig. 2). The exposed CuO surface area determined by this method, and other relevant properties of the BASF sample K3-110 are listed in Table 1.

Fig. 3 shows FESEM/EDXS data of a fresh, untreated $CuO/ZnO/Al_2O_3$ catalyst. They showed that the majority of the CuO and ZnO appear in large agglomerates in the order of 5 μm in size. Additional structures existed consisting of $Al_2O_3$ and carbon added as stabilizers and supports. It appeared that the bulk CuO/ZnO amalgamations are relatively separated from the $Al_2O_3$ and the carbon filler (Fig. 3a–d). It is well known that $Al_2O_3$ and carbon have little activity for methanol oxidation at the lower temperatures representative of this study. It is likely then, that either CuO or ZnO or both are the active phases with the other components being inert.

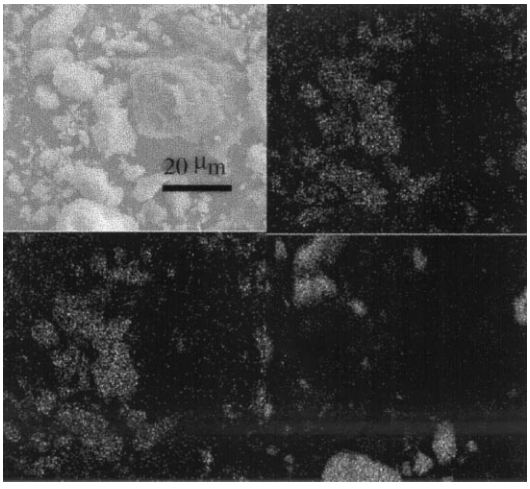


Fig. 3. SEM data of fresh $CuO/ZnO/Al_2O_3$, 1000x magnification, clockwise from top: (a) SEM image, (b) EDXS Cu, (c) EDXS Zn, (d) EDXS Al.

### 3.2. Reaction under oxidizing conditions

It was determined previously that under differential conditions, a fresh sample of $CuO/ZnO/Al_2O_3$ was active primarily for the oxidation of methanol with a $CO_2/H_2O$ product ratio of 1:2 [18]. Small amounts of formic acid was also detected as a primary product, while minor $H_2$ production was determined to occur as a result of secondary reactions (Fig. 4). Prereduction of the catalyst, under conditions where bulk reduction of the copper was assured, revealed that reoxidization occurred when subjected to differential oxygen conversions and dominant oxidation selectivity was again observed. The product distribution under differential conditions was dramatically different from selectivities observed under complete $O_2$ conversion conditions. Once $O_2$ conversion is complete, it was found that the bulk copper phase is completely reduced to $Cu^0$ and $H_2$ becomes a dominant reaction product.

The reaction kinetics were determined for methanol and $O_2$ conversions less than 3% and 20%, respectively, and a temperature range of 180–225°C.

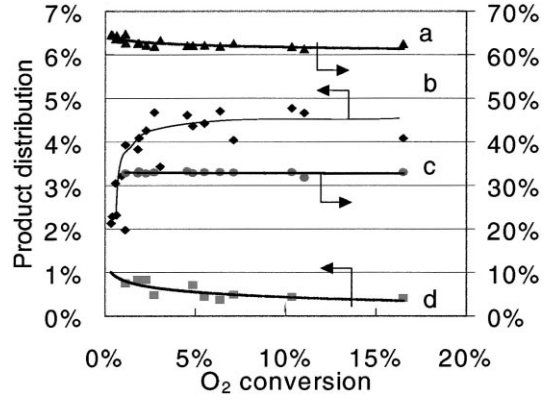


Fig. 4. Product distribution as a function of $O_2$ conversion for the OMR reaction: (a) $H_2O$, (b) $H_2$, (c) $CO_2$, (d) HCOOH.

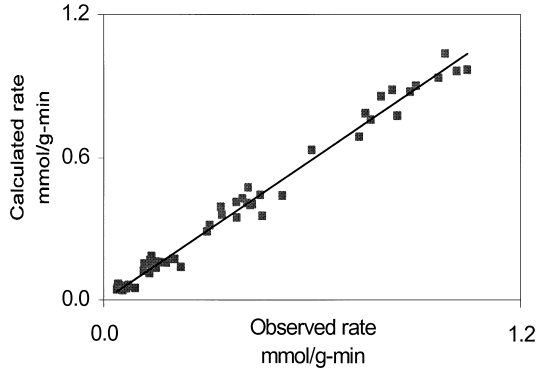


Fig. 5. Correlation plot for reaction rate data for the temperature ranges of 180°C to 225°C.

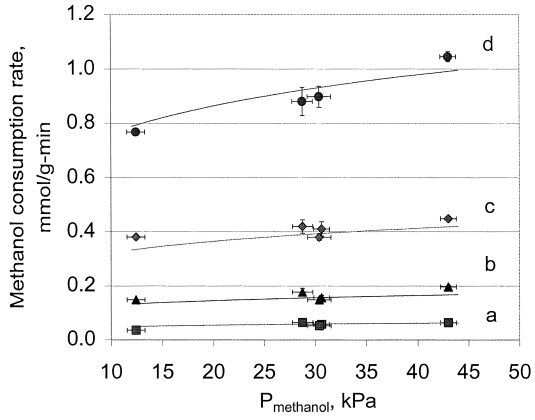


Fig. 7. Dependence of methanol consumption rate on $P_{methanol}$, (a) $T = 180$°C, (b) $T = 195$°C, (c) $T = 210$°C, (d) $T = 225$°C.

The rate of methanol disappearance can be represented in the Power-Law form (Eq. (6)).

$$-R_{CH_3OH} = A_o \exp\left(\frac{-E_a}{RT}\right) \frac{P_{methanol}^{0.18} P_{O_2}^{0.18}}{P_{H_2O}^{0.14}}. \qquad (6)$$

The correlation plot of the observed versus calculated rates, as well as the dependence of the rate on $P_{O_2}$, $P_{CH_3OH}$, and $P_{H_2O}$ are shown in Figs. 5–8. The inhibitory influence of steam was attributed to competitive adsorption of water with $O_2$ and/or methanol. It is also possible that the high concentration of water in the gas phase simply inhibits desorption of surface bound water produced during methanol oxidation. The positive order of the $O_2$ partial pressure with reaction rate is common for oxidation reactions. If the reaction of methanol reduces the $Cu^{+2}$ to $Cu^{+}$ or $Cu^{0}$, which is reoxidized by oxygen, then a positive order on oxygen is not unexpected. However, direct oxidation of adsorbed methanol with adsorbed oxygen would also suggest a positive order in oxygen.

The activation energy as a function of component partial pressure are shown in Figs. 9–11. The activation energy for the reaction was found to be $115 \pm 6$ kJ/mol and the pre-exponential factor to be $6.0 \pm 0.2 \times 10^8$ mol $(\text{min} \cdot \text{gcat} \cdot \text{kPa}^{0.22})^{-1}$. No statistical trend was observed in the activation energy as a function of $O_2$ or methanol partial pressure suggesting a power-law kinetic expression fits the data

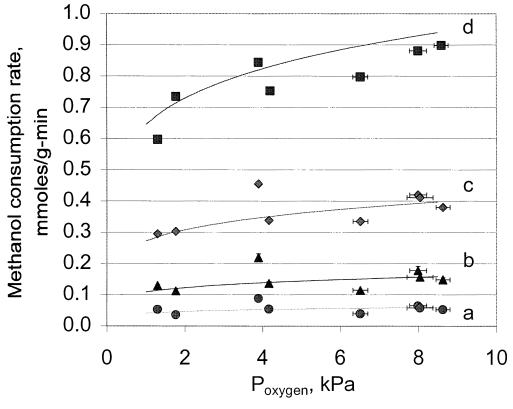


Fig. 6. Dependence of methanol consumption rate on $P_{oxygen}$, (a) $T = 180$°C, (b) $T = 195$°C, (c) $T = 210$°C, (d) $T = 225$°C.

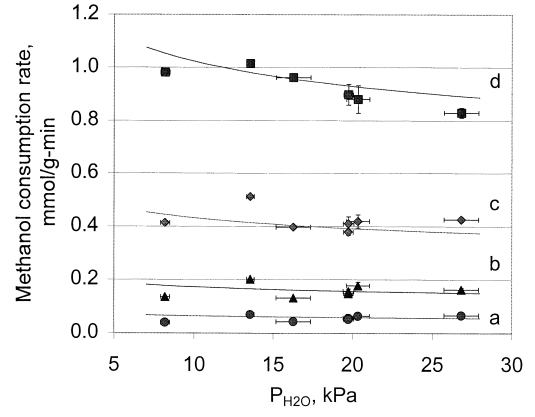


Fig. 8. Dependence of methanol consumption rate on $P_{steam}$, (a) $T = 180$°C, (b) $T = 195$°C, (c) $T = 210$°C, (d) $T = 225$°C.

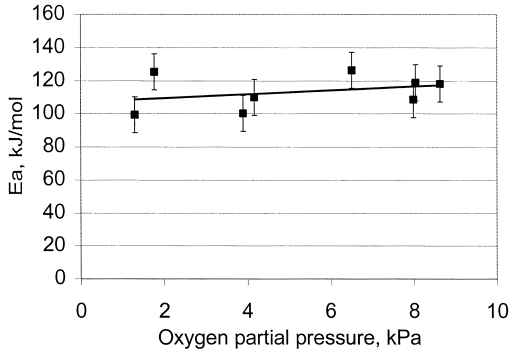


Fig. 9. Dependence of activation energy on oxygen partial pressure.

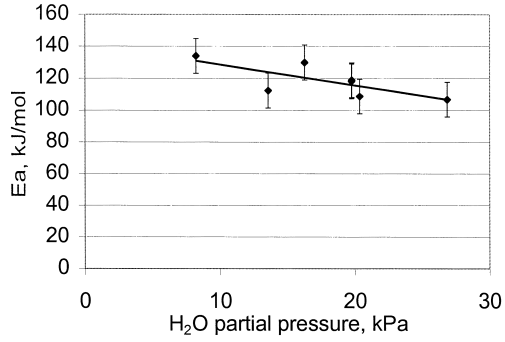


Fig. 11. Dependence of activation energy on steam partial pressure.

appropriately. However, the activation energy varied more significantly with water partial pressure, ranging from 134 kJ/mol at 8.2 kPa to nearly 106 kJ/mol at 27 kPa. A possible explanation is that as the surface coverage of water increases, there is a monotonic decrease in the heat of adsorption. Since adsorbed water suppresses the reaction, a lower heat of adsorption lowers the apparent activation energy of the reaction. This is consistent with the findings that, for methanol synthesis, the heat of adsorption of water over a reduced $Cu/ZnO/Al_2O_3$ is a linear decreasing function with surface coverage [30].

### *3.3. Deactivation of $CuO/ZnO/Al_2O_3$ under oxidizing conditions*

As shown previously [18], $CuO/ZnO/Al_2O_3$ was found to deactivate with time-on-stream at 225°C (Fig. 12). The initial activity for fresh samples pretreated in various atmospheres are shown in Table 2. The results show that treatment with $N_2$ or air and steam at 225°C did not cause deactivation of the $CuO/ZnO/Al_2O_3$ sample. However, treatment at 350°C caused significant deactivation independent of the atmosphere. Samples treated in steam at 350°C showed the most deactivation, with only ~33% of the activity remaining. Preliminary evidence suggests that the rate of deactivation decreased with increasing $P_{O_2}$.

In order to test whether deactivation is associated with reduction of the CuO in the sample, TPR was performed on a sample deactivated to 33% of original activity. As shown in Fig. 13, negligible difference in the amount of reducible CuO was observed compared with a fresh, undeactivated sample. $H_2$ consumption was determined to be $0.9 \pm 0.05$

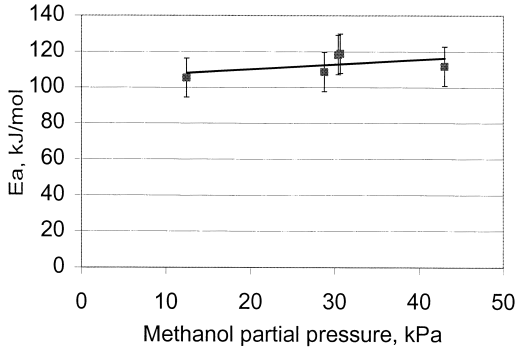


Fig. 10. Dependence of activation energy on methanol partial pressure.

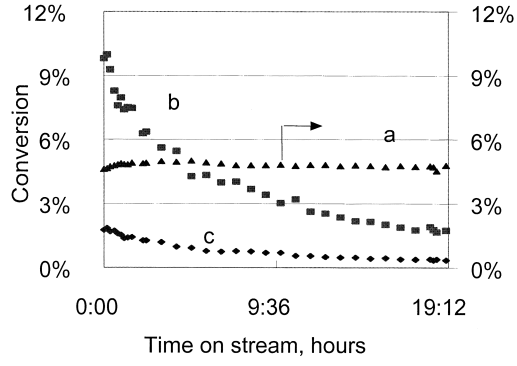


Fig. 12. Deactivation profile for $CuO/ZnO/Al_2O_3$ under oxidizing conditions, (a) mole % $H_2$ in product, (b) $O_2$ conversion, (c) $CH_3OH$ conversion.

Table 2
Reaction rates with deactivation treatments for various $CuO/ZnO/Al_2O_3$ samples

| Deactivation treatment | Methanol conversion at 225°C ($W/F_{methanol} = 11.8 \pm 0.7$) | Initial rate | |
|---|---|---|---|
| | | Mmol/g catalyst min | Molecules/CuO site min |
| Fresh, no treatment | $0.9 \pm 0.03\%$ | $0.78 \pm 0.05$ | $5.5 \pm 0.6$ |
| $N_2$ and steam at 225°C, for 3 h | $1.6 \pm 0.11\%$ | $1.20 \pm 0.10$ | $4.7 \pm 0.5$ |
| $N_2$ and steam at 225°C, for 24 h | $1.1 \pm 0.07\%$ | $0.93 \pm 0.08$ | $5.5 \pm 0.6$ |
| Air and steam at 225°C, for 24 h | $1.5 \pm 0.13\%$ | $1.34 \pm 0.14$ | $6.3 \pm 0.7$ |
| $N_2$ only at 350°C, for 24 h | $0.6 \pm 0.03\%$ | $0.50 \pm 0.04$ | $4.4 \pm 0.5$ |
| $N_2$ and steam at 350°C, for 24 h | $0.4 \pm 0.02\%$ | $0.34 \pm 0.03$ | $2.6 \pm 0.3$ |
| Air and steam at 350°C, for 24 h | $0.3 \pm 0.02\%$ | $0.26 \pm 0.02$ | $4.6 \pm 0.8$ |

mol/mol CuO for the deactivated sample compared with $0.8 \pm 0.05$ mol/mol CuO for the fresh sample. The XRD patterns of some deactivated samples are shown in Fig. 14. The XRD pattern of the fresh, oxidized copper catalyst (plot a) shows broad peaks at 13.1°, 24.2°, and 28.1° $2\theta$ indicative of the minerals hydrozincite and malaquite. These peaks disappeared after treating the samples in $N_2$ and steam at 225°C without affecting catalytic activity. Treatment of the catalyst at 225°C caused a slight sharpening of the CuO peak at 38.8° $2\theta$ and the ZnO peak at 31.8° $2\theta$. The sharpening was most noticeable after treatment at 350°C, where substantial deactivation was observed.

Fig. 15 shows the variation of catalytic activity, measured at 225°C under similar space times, with average CuO and ZnO crystallite size, as estimated by the Scherrer equation. While catalytic activity decreased with increasing CuO crystallite size, the dependence on ZnO was much less obvious. Interestingly, the fresh catalyst is much less active than predicted by the CuO crystallite size. The major difference between the fresh sample and a mildly treated sample ($N_2$/water at 225°C for 24 h) are the dramatic increase in the ZnO particle size followed by the disappearance of the mineral phases. This suggests that perhaps the CuO/ZnO mineral phases discussed previously potentially inhibit the exposure of the active CuO site. TPR evidence also supported this finding. While there was no difference in the quantity of the CuO reduced (Fig. 13b and c) the sample of mild treatment showed a lower $T_m$ over the fresh, untreated $CuO/ZnO/Al_2O_3$. It is, therefore, postulated that a slight thermal treatment is necessary to cause the decomposition of the mineral phases into more active, separate constituents.

In order to confirm that deactivation was a result of thermal sintering of CuO, the surface area of CuO

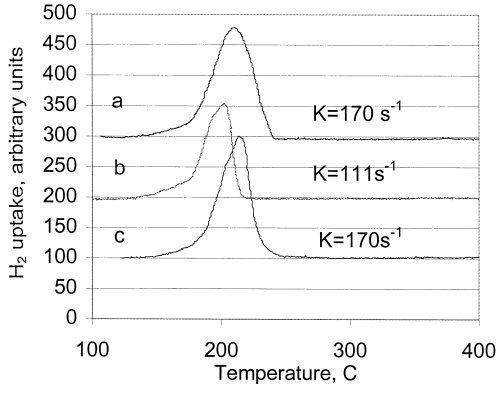


Fig. 13. TPR plots for: (a) fresh $CuO/ZnO/Al_2O_3$, (b) $CuO/ZnO/Al_2O_3$ treated in $N_2$ and steam at 225°C for 3 hrs, (c) sample with 67% deactivation.

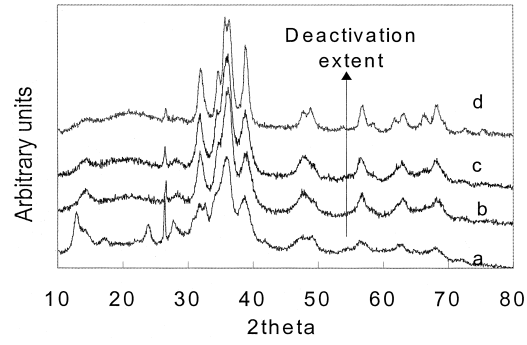


Fig. 14. XRD diffraction patterns for differing extents of deactivation. (a) Fresh catalyst, (b) 3 hr $N_2$/Steam @225°C, (c) 24 hr $N_2$/steam @225°C, (d) 24 hr $N_2$/steam @350°C.

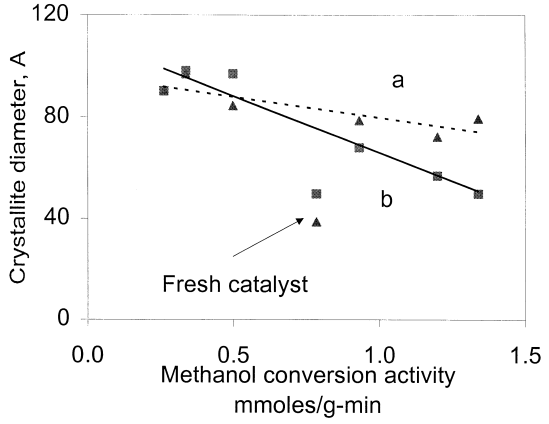


Fig. 15. Dependence of average CuO crystallite size on methanol consumption rate, measured at 225°C and $W/F_{methanol} = 11.8 +/-0.7$ (W[ = ] weight of catalyst in grams, F[ = ] flow of methanol in mole/min), (a) ZnO, (b) CuO.

was measured using the technique discussed earlier. The dependence of the CuO surface area on the methanol conversion activity is shown in Fig. 16. As with Fig. 14, a direct correlation was observed, suggesting that the majority or all of the oxidizing activity is due to exposed CuO. The turnover frequency was calculated to be $4.7 \pm 1$ molecules $\cdot$ CuO site$^{-1} \cdot$ min$^{-1}$ for all of these catalysts. These data strongly suggest that the decrease in methanol oxidation activity over an oxidizing catalyst is primarily due to a decrease in the dispersion of the active CuO phase. It becomes obvious then that, in order to maintain a high methanol oxidizing activity, it is essential to retain high CuO dispersion. ZnO, however, is relatively resistant to sintering under the conditions experienced during methanol oxidation. This supports the conclusion that ZnO is not significantly involved during the oxidation of methanol.

The production of $H_2$ during oxidization of methanol allows some conclusions to be drawn about potential reaction networks for the oxidative region during methanol reforming. As mentioned previously, $CuO/ZnO/Al_2O_3$ has been shown to deactivate under oxidizing conditions, but with no change in product selectivity [18]. As a result, $H_2$ production can be assumed to be produced on the same site as methanol oxidation. One possibility is that it is formed by the decomposition of formic acid into $H_2$ and $CO_2$ (Eq. (8)). In the presence of $O_2$, methanol can be oxidized to formic acid, which has been detected by GC. Under low $O_2$ conversion conditions, sufficient $O_2$ is still available, favoring the complete oxidation of formic acid to $CO_2$ and $H_2O$ (Eq. (8)). However, as $O_2$ conversion increases, the decomposition pathway (Eq. (9)) becomes more significant relative to Eq. (8), consistent with experimental data showing $H_2$ as a secondary product (Fig. 3). Because they are so energetically favorable, Eqs. (7) and (8) are likely to be very labile relative to Eqs. (9) and (10). As a result, at lower $O_2$ conversions, higher formic acid production would be expected, increasing the likelihood for desorption of formic acid (Eq. (10)) [31–34].

$$CH_3OH + O_2 = HCOOH_{(ads)} + H_2O_{(ads)} \quad (7)$$

$$HCOOH_{(ads)} + 1/2O_{2(ads)} = CO_2 + H_2O \quad (8)$$

$$HCOOH_{(ads)} = CO_2 + H_2 \quad (9)$$

$$HCOOH_{(ads)} = HCOOH_{(g)} \quad (10)$$

Another possibility is that $H_2$ is formed by the water gas shift reaction (WGS Eq. (11)). However, for WGS to have a significant role in $H_2$ production, CO would need to be at least as high as the equilibrium concentration under these conditions, which is in the order of 1 ppm. To detectable limits of approximately 50 ppm, no CO was observed over the range of this study. $H_2$ formation from methanol decomposition (Eq. (12)) is also unlikely, because no

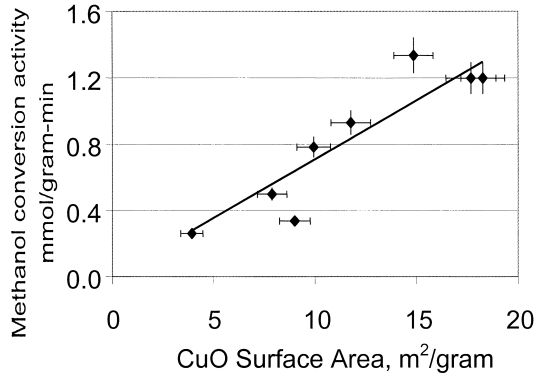


Fig. 16. Dependence of methanol consumption rate, measured at 225°C and $W/F_{methanol} = 11.8 +/-0.7$(W[ = ] weight of catalyst in grams, F[ = ] flow of methanol in mole/min), on exposed CuO surface area.

CO was detected. However, rapid CO removal by oxidation to $CO_2$ cannot be ruled out in either case.

$$H_2O + CO = H_2 + CO_2 \quad (11)$$

$$CH_3OH = CO + 2H_2 \quad (12)$$

## 4. Conclusions

Differential kinetics for the oxidation of methanol over $CuO/ZnO/Al_2O_3$ has been shown to be successfully modeled by a Power-Law expression. Under these conditions, products of complete combustion are dominant. By increasing the reaction temperature slightly, a non-linear increase in the $O_2$ consumption is observed followed by a complete reduction of the copper oxide to metallic copper. Under these conditions, the dominate reaction is steam reforming. As a result, an operational $CuO/ZnO/Al_2O_3$ catalyst bed can be partitioned into two regions with a transition region in between. Under differential conditions, the entire catalyst bed remains oxidized with activity primarily for the oxidation of methanol to water and carbon dioxide. Under typical operation conditions of high oxygen and methanol conversions, this region of oxidized catalyst is short. Methanol oxidation proceeds in this region until the oxygen is practically all consumed. The heat of reaction causes the catalyst temperature to rise rapidly. After this region, the atmosphere is substantially reducing resulting in the autothermal reduction of the catalyst with a prominent shift to methanol reforming as the dominant reaction.

Deactivation under oxidizing conditions has been shown to be due to a decrease in exposed CuO. As the sample deactivates with time-on-stream, the CuO surface area was found to vary linearly with the methanol oxidation rate. Consequently, the activity was observed to decrease with increasing CuO crystallite size. Similar trends were not observed with ZnO. This data is fairly conclusive that CuO is the principal active phase responsible for methanol combustion in the presence of gas phase $O_2$. Temperature appears to be the most significant cause for CuO sintering. Despite attempts to minimize hot spots in the catalyst by inclusion of diluents, the temperature control was still not sufficient such that local heating occurs at high reaction rates. Consequently, accelerated sintering of CuO occurs at the hot spots. Therefore, under typical operating conditions, the catalyst near the reactor entrance, which is responsible for methanol oxidation, will deactivate with time-on-stream. Thus, the oxidation section lengthens down the bed with time. The point where the catalyst is reduced also propagates down the bed resulting in an overall decrease in the bed efficiency to produce $H_2$. Practically all of the $H_2$ produced occurs over copper metal in the latter section of the reactor where steam reforming of methanol is the dominant reaction.

Supported copper oxide catalysts have been shown to be highly active for the OMR reaction. The above results strongly suggest that the catalyst performs multiple functions, the activity of which is primarily determined by the oxidation state of the copper. Because of the bifunctional aspect of this system, it is possible that other catalysts may be more effective for the overall generation of hydrogen. This could be a subject of future investigations.

## Acknowledgements

Support of this work by the Argonne National Laboratory of the Department of Energy is gratefully acknowledged.

## References

[1] US Congress, Office of Technology Assessment, OTA-ETI-638, Washington, DC, US Gov. Printing Office, Sept., 1995.
[2] US Congress, Office of Technology Assessment, OTA-ETI-589, Washington, DC, US Gov. Printing Office, July, 1994.
[3] US Congress, Office of Technology Assessment, OTA-O-412, Washington, DC, US Gov. Printing Office, July, 1989.
[4] Congressional Research Service, Environmental and Natural Resource Policy Division, June 3, 1992.
[5] R. Kumar, S. Ahmed, M. Krumpelt, K.M. Myles, Argonne National Laboratory Report, ANL-92/31, Argonne, IL, USA, 1992.
[6] R. Kumar, S. Ahmed, M. Krumpelt, 1996 Fuel Cell Seminar Program and Abstracts, 1996, p. 750.
[7] C.J. Jiang, D.L. Trimm, M.S. Wainwright, N.W. Cant, Appl. Catal. 93 (1993) 245.
[8] C.J. Jiang, D.L. Trimm, M.S. Wainwright, N.W. Cant, Appl. Catal. 97 (1993) 145.

[9] N. Takezawa, N. Iwasa, Catal. Today 36 (1997) 45.
[10] B.A. Peppley, J.C. Amphlett, L.M. Kearns, R.F. Mann, Appl. Catal. 179 (1999) 21.
[11] B.A. Peppley, J.C. Amphlett, L.M. Kearns, R.F. Mann, Appl. Catal. 179 (1999) 31.
[12] T.J. Huang, S.W. Wang, Appl. Catal. 24 (1986) 287.
[13] T.J. Huang, S.L. Chren, Appl. Catal. 40 (1988) 43.
[14] I.E. Wachs, R.J. Madix, J. Catal. 53 (1978) 208.
[15] L. Alejo, R. Lago, M.A. Pena, J.L.G. Fierro, Appl. Catal. 162 (1997) 281.
[16] M.L. Cubeiro, J.L.G. Fierro, J. Catal. 179 (1998) 150.
[17] M.L. Cubeiro, J.L.G. Fierro, Appl. Catal. 168 (1998) 307.
[18] T.L. Reitz, S. Ahmed, M. Krumpelt, R. Kumar, H.H. Kung, Proc. 12th Int. Cong. Catal., accepted for publication.
[19] R.M. Dell, F.S. Stone, P.F. Tiley, Trans. Faraday Soc. 49 (1953) 195.
[20] R.M. Dell, F.S. Stone, P.F. Tiley, Trans. Faraday Soc. 49 (1953) 201.
[21] J. Osinga, B.G. Linsen, W.P. Van Beek, J. Catal. 7 (1967) 277.
[22] K.J. Soerensen, N.W. Cant, Catal. Lett. 33 (1995) 117.
[23] A. Dandekar, M.A. Vannice, J. Catal. 178 (1998) 621.
[24] D.A.M. Monti, A. Baiker, J. Catal. 83 (353) (1983).
[25] P. Malet, A. Caballero, J. Chem. Soc., Faraday Trans. 84 (2369) (1988).
[26] G. Fierro, M. Lo Jacono, M. Inversi, P. Porta, R. Lavecchia, F. Cioci, J. Catal. 148 (1994) 709.
[27] G. Fierro, M. Lo Jacono, M. Inversi, P. Porta, F. Cioci, R. Lavecchia, Appl. Catal. 137 (1996) 327.
[28] A.F. Wells, Structural Organic Chemistry, 3rd edn., Oxford Univ. Press, 1962, 868 pp.
[29] J.J.F. Scholten, J.A. Konvalinka, Trans. Faraday Soc. 65 (1969) 2465.
[30] J. Skrzypek, J. Sloczynski, S. Ledakowiez, Methanol Synthesis, Polish Scientific Publishers, Warsaw, 1994, ISBN 83-01-11490-8.
[31] N.W. Cant, S.P. Tonner, D.L. Trimm, M.S. Wainwright, J. Catal. 91 (1985) 197.
[32] R. Ramos, G. Ruiz, M.L. Rojas, J.L.G. Fierro, Appl. Catal. 68 (1991) 217.
[33] L. Domokos, T. Katona, A. Molnar, A. Lovas, Appl. Catal. 142 (1996) 151.
[34] S. Sato, M. Iijima, T. Nakayama, T. Sodesawa, F. Nozaki, J. Catal. 169 (1997) 447.